Experimental Eye Research 207 (2021) 108581

Contents lists available at ScienceDirect

Experimental Eye Research

journal homepage: www.elsevier.com/locate/yexer

A novel 3D culture model of fungal keratitis to explore host-pathogen interactions within the stromal environment

Marina E. Brown [a,1], Micaela L. Montgomery [b,1], Manali M. Kamath [b], Sarah Nicholas [d,e], Yutao Liu [c], Dimitrios Karamichos [d,e,f], Kevin K. Fuller [a,b,*]

[a] Department of Ophthalmology, University of Oklahoma Health Sciences Center, Oklahoma City, OK, USA
[b] Department of Microbiology and Immunology, University of Oklahoma Health Sciences Center, Oklahoma City, OK, USA
[c] Department of Cellular Biology and Anatomy, Augusta University, Augusta, GA, USA
[d] North Texas Eye Research Institute, University of North Texas Health Science Center, 3500 Camp Bowie Blvd, Fort Worth, TX, 76107, USA
[e] Department of Pharmaceutical Sciences, University of North Texas Health Science Center, 3500 Camp Bowie Blvd, Fort Worth, TX, 76107, USA
[f] Department of Pharmacology and Neuroscience, University of North Texas Health Science Center, 3500 Camp Bowie Blvd, Fort Worth, TX, 76107, USA

ARTICLE INFO

Keywords:
Fungal keratitis
Corneal fibroblasts
Keratocytes
Corneal inflammation
Matrix metalloprotease
Fusarium

ABSTRACT

Fungal keratitis (FK) pathology is driven by both fungal growth and inflammation within the corneal stroma. Standard *in vitro* infection models– involving co-culture of the pathogen and the corneal cells in tissue culture medium– are sufficient to probe host responses to the fungus; however, they lack the physiological structure and nutrient composition of the stroma to accurately study fungal invasiveness and metabolic processes. We therefore sought to develop a culture model of FK that would allow for both host and fungal cell biology to be evaluated in parallel. Towards this end, we employed a previously described system in which primary human cornea fibroblasts (HCFs) are cultured on transwell membranes, whereupon they secrete a three-dimensional (3D) collagen matrix that resembles the human stroma. We demonstrated that two common mold agents of FK, *Fusarium petroliphilum* and *Aspergillus fumigatus*, penetrated into these constructs and caused a disruption of the collagen matrix that is characteristic of infection. HCF morphology appeared altered in the presence of fungus and electron microscopy revealed a clear internalization of fungal spores into these cells. Consistent with this apparent phagocyte-like activity of the HCFs, mRNA and protein levels for several pro-inflammatory cytokines/chemokines (including TNFα, IL-1β, IL-6, and IL-8) were significantly upregulated compared to uninfected samples. We similarly found an upregulation of several HCF metalloproteases (MMPs), which are enzymes that breakdown collagen during wound healing and may further activate pro-inflammatory signaling molecules. Finally, several fungal collagenase genes were upregulated during growth in the constructs relative to growth in tissue culture media alone, suggesting a fungal metabolic shift towards protein catabolism. Taken together, our results indicate that this 3D-stromal model provides a physiologically relevant system to study host and fungal cell pathobiology during FK.

1. Introduction

Fungal keratitis (FK) is an infection of the cornea and a significant source of ocular morbidity and unilateral blindness worldwide (Thomas and Kaliamurthy, 2013). Two major risk factors for FK include corneal trauma caused by vegetative debris and contact lens wear (Saha et al., 2009; Cheung et al., 2016). In both contexts, the molds *Fusarium* and *Aspergillus* have emerged as predominant agents of infection, likely due their ubiquity in the soil, on vegetation, and even within fresh-water plumbing systems (Rosa et al., 2009; Bharathi et al., 2007; Short et al., 2013). *Fusarium* species, for example, were the sole agents of FK in a multi-country outbreak (included the United States) associated with a commercial lens cleaning solution (Chang et al., 2016). Regardless of the infectious route or etiology however, medical intervention in the form of topical antifungals fails in up to 50% of FK cases, resulting in the need for corneal transplantation or even enucleation if the infection spreads

* Corresponding author. Departments of Ophthalmology and Microbiology & Immunology, University of Oklahoma Health Sciences Center, Dean McGee Eye Institute, 608 Stanton L. Young Blvd., USA.
E-mail address: Kevin-Fuller@ouhsc.edu (K.K. Fuller).
[1] authors contributed equally to this work.

https://doi.org/10.1016/j.exer.2021.108581
Received 12 November 2020; Received in revised form 16 March 2021; Accepted 10 April 2021
Available online 15 April 2021
0014-4835/© 2021 The Authors. Published by Elsevier Ltd. This is an open access article under the CC BY-NC-ND license (http://creativecommons.org/licenses/by-nc-nd/4.0/).

to intraocular compartments (Mundra et al., 2019). A better understanding of FK pathobiology is therefore required to fuel the development of novel and more efficacious treatment modalities.

FK occurs when a breakdown in corneal epithelial integrity allows the fungus to access and grow within the central stroma. The stroma comprises about 90% of the corneal thickness and accounts for the overall transparency of the tissue due to its avascularity, paucity of resident cells and careful assembly of collagen fibrils (Spadea et al., 2016; Doughty and Jonuscheit, 2019). Fungal growth is inherently damaging to the stoma as the organism secretes copious amounts of hydrolytic enzymes (collagenases) that may directly damage the collagen extracellular matrix (ECM) (Zhu et al., 1990). Just as damaging, however, is the resulting host response. The massive influx of neutrophils from the periphery alters the refractive index of stroma, leading to corneal opacification and acute visual impairment (Leal and Pearlman, 2012). Though ostensibly important for fungal clearance, neutrophils further secrete matrix metalloproteases (MMPs), which are zinc-binding collagenases that can further exacerbate stromal breakdown and promote fungal proliferation, corneal melt and long-term corneal scarring (Taylor et al., 2016). MMPs further cleave and process pro-inflammatory molecules, such as IL-1β, thus propagating the inflammatory cascade (Sivak and Fini, 2002). Both the general induction of neutropenia by cyclophosphamide and the specific blocking of MMPs with neutralizing antibodies mitigate disease development in murine models of fungal or bacterial keratitis, thereby underscoring the significance of the host response in keratitis pathology (Leal et al., 2010; McClellan et al., 2006; Gao et al., 2015). Accordingly, host cell populations and signaling pathways that trigger this inflammatory/fibrotic response may represent ideal targets for FK intervention.

Stromal keratocytes are mesenchymal-derived, non-contractile, dendritic-shaped cells distributed across the stroma. These cells exist in a largely quiescent state, slowly producing crystallins, collagens, proteoglycans, and other products that are critical in maintaining the stromal ECM and corneal transparency. Following corneal injury, or upon exposure to serum *in vitro*, keratocytes differentiate into fibroblasts, which are characterized by their increased size, spindle shape, increased phagocytic activity, and migratory action (Sato et al., 2019; Fujita et al., 1987; Fukuda et al., 2017; Myrna et al., 2009). Once at the site of stromal damage, fibroblasts remodel the ECM by secreting both MMPs as well as collagen sub-types that may heal the wound but result in scarring due to irregular collagen deposition (Sugioka et al., 2018). In addition, macrophage-like gene expression is induced following the keratocyte-to-fibroblast transition, including an upregulation of mannose receptor type 1, chemokine ligands, CD68 (typically only expressed on monocytes and macrophages), and complement component pathway genes (Chakravarti et al., 2004).

Corneal fibroblasts have been further implicated as modulators of inflammation and corneal damage in the context of microbial keratitis. First, the cells secrete pro-inflammatory cytokines, including the chemokine MCP-1 and IL-8 (aka CXCL8), in the presence of either bacterial lipopolysaccharide (LPS) or peptidoglycan. They also produce various pro-MMPs that are cleaved and activated by bacterial-derived proteases (Fukuda et al., 2005, 2017). Similar results are seen in the presence of fungal antigen, as Nomi et al. demonstrated that cultured corneal fibroblasts secrete IL-6 and IL-8 when challenged with zymosan (purified β-glucan)-coated beads; this response appears to be mediated through the MAP kinase and NF-kB signaling pathways (Nomi et al., 2010). Li and colleagues demonstrated a similar pro-inflammatory response when immortalized human corneal fibroblasts (HCFs) were stimulation with heat-killed *A. fumigatus* hyphae. Interestingly, the magnitude of the response to hyphal challenge could be attenuated by pre-treating the fibroblasts with lipopolysaccharide and zymosan, which are ligands for TLR 4 and TLR2, respectively (Li et al., 2013). In addition to providing insight into signaling mechanism, the studies suggest that corneal fibroblasts could serve as targets for anti-inflammatory treatment in FK.

Interrogating how specific host cells interact with fungi during infection may be challenging *in vivo* due to the presence of numerous corneal cell types, particularly after inflammation sets in shortly after fungal inoculation. *In vitro* models, such as those used in the above-described fibroblast-fungal studies, bypass this problem (Montgomery and Fuller, 2020). However, standard culture models fall short because they lack important features of the stroma, in particular the collagen matrix in which the host-pathogen interaction takes place. Karamichos and colleagues demonstrated that primary HCFs cultured on a polycarbonate transwell membrane secrete a collagen ECM that resembles the composition of a healthy corneal stroma (Karamichos et al., 2007, 2010); Sharif et al., 2018; McKay et al., 2019; Priyadarsini et al., 2016). We reasoned that these three-dimensional (3D) constructs would serve as a valuable *in vitro* model for FK for several reasons. Not only can HCF activity be probed as they are the only host cell present, but the fungal penetration and damage to the collagen ECM can also be evaluated. Moreover, the presence of ECM components, e.g. collagen, may further influence fungal metabolism such that it more closely mimics that of live infection.

In this study, we challenged the 3D-stromal constructs with two common mold agents of FK, *Fusarium petroliphilum* and *Aspergillus fumigatus*, and found they could both penetrate through and damage the stromal ECM. We also found that HCFs phagocytosed fungal conidia and, in agreement with previous studies, expressed both pro-inflammatory and matrix-remodeling genes/proteins. Finally, we demonstrate several *A. fumigatus* collagenase genes are upregulated when grown in the constructs relative to culture in tissue culture medium. This suggests that the presence of the stomal ECM does influence fungal gene expression, and that this model can be useful for probing both host and fungal biology during FK.

2. Materials and methods

2.1. Culture of primary human corneal fibroblasts

Human corneas were obtained from the National Development and Research Institute (NDRI) and fibroblasts were isolated as described by Guo et al. (2007). Briefly, the corneal epithelium and endothelium were scraped off with a razor blade and the remaining stroma was sectioned into small 2 × 2 mm squares that were placed in T25 flasks and allowed to adhere. These explants were cultured with Eagle's Minimum Essential Media (EMEM: ATCC; Manassas, VA) that contained 10% fetal bovine serum (FBS: ATCC) and 1% antibiotic and antimycotic 100X (AA: Life Technologies, Grand Island, NY). Cultures were incubated at 37 °C, 5% CO_2 for 1–2 weeks or until 100% confluent, and were passaged following trypsin digestion.

2.2. Construct assembly

1.0×10^6 fibroblasts/ml EMEM were seeded onto a polycarbonate transwell membrane insert with 0.4 μm pores for a conventional 6-well tissue culture plate (Corning Costar; Corning Incorporated, Corning, NY, USA). Cells were incubated for 24 h in EMEM. After 24 h, a routine media change was performed every 48 h for 4 weeks with supplemented EMEM that contained 1 μM 2-O-α-D-glucopyranosyl-L-ascorbic acid (American Custom Chemicals Corporation, San Diego, CA), 10% FBS, and 1% AA.

2.3. Preparation of fungal inoculum and infection of the stromal constructs

The *Fusarium petroliphilum* strain used in this study is an FK isolate previously described (Lightfoot and Fuller, 2019). To generate the inoculum, *F. petroliphilum* spores (microconidia) were inoculated into YPD broth and incubated for 2–3 days at 30 °C, shaking at 200 RPM. Microconidia were harvested by passage through Miracloth (EMD Millipore) and pelleted by centrifugation at 3500 RPM. The spore pellets

were then washed in PBS twice and ultimately resuspended in PBS and adjusted to a density of 6.74×10^4 conidia/mL. *Aspergillus fumigatus* was cultured on solid glucose minimal medium (GMM) containing 1% glucose and ammonium tartrate for 48 h at 35 °C. Conidia were collected by washing the surface with PBS and filtering through miracloth (Millipore), followed by two washes in PBS. The conidia were enumerated using a hemocytometer and adjusted to a density of 6.74×10^4 conidia/mL.

72 h preceding the inoculation, the EMEM medium in the upper and lower chambers of the plates were replaced with EMEM containing no antibacterial/antimycotic. On the day of inoculation, media in the top chamber was removed and the constructs were washed twice with 1 ml of PBS. 750 μl of fungal inoculum was overlaid on the constructs, giving a final inoculum 5×10^4 conidia in the top chamber of the transwell system. The bottom chamber was replaced with fresh EMEM containing no FBS and no antibacterial/antimycotic. Samples were incubated undisturbed for their indicated time point at 35 °C and 5% CO_2.

2.4. RNA isolation and RNA-seq from stromal constructs

The artificial stroma and fungal inoculum were peeled from the polycarbonate membrane and placed in a 1.5 ml microcentrifuge tube with 0.5 mm diameter glass beads and tissue was homogenized using QIAGEN TissueLyser LT at 50 oscillations/s for two 30 s cycles. RNA extraction was performed following the manufacturer's protocol for QIAGEN RNeasy Mini Kit (QIAGEN Science, Germantown, Maryland). For RNA-sequencing, 200 ng total RNA from all subjects were used to prepare sequencing libraries with the TaKaRa SMARTer Stranded RNA-Seq kit after ribosomal RNA depletion using the RiboGone - Mammalian kit from TaKaRa (TaKaRa Bio USA, Inc., Mountain View, CA, USA). Briefly, the RiboGone-Mammalian kit removes ribosomal RNA (rRNA) and mitochondrial RNA (mtRNA) sequences from human total RNA samples based on hybridization and RNase H digestion that specifically depletes 5 S, 5.8 S, 18 S, and 28 S nuclear rRNA sequences, as well as 12 S mtRNA sequences. The rRNA-depleted total RNA was reverse-transcribed to synthesize the first-strand complementary (c) DNA followed by PCR amplification using universal forward PCR primer and reverse PCR indexing primer set. Purified RNA-Seq library was validated using the Agilent 2100 Bioanalyzer with Agilent's High Sensitivity DNA Kit (Agilent, Santa Clara, CA, USA). Pooled RNA-Seq libraries were sequenced with paired-end 75-bp reads using an Illumina NextSeq sequencer with high output v2 (Illumina, Inc., San Diego, CA, USA) at the Georgia Cancer Center Integrated Genomics Core of Augusta University. After quality check and control with all sequencing reads, demultiplexed reads were aligned by TopHat31 using paired-end reading with the approximation of the median library size. Counts of sequencing reads were normalized using Cufflinks in fragments per kilo bases and millions reads (FPKM). After normalization, we annotated the transcripts with a gene transcript file from Ensembl database at the gene isoform level. We performed differential expression analysis using the Cuffdiff package.

2.5. Protein isolation and measurement from stromal constructs

3D constructs were washed with 1 mL 1X PBS and then, using a spatula, were gently scraped off of the membrane and placed in a 2 mL tube containing a 6.35 mm metal ball, T-PER (ThermoScientific, Ref. #78510), and Calbiochem protease inhibitor cocktail set I (Millipore Sigma, Cat. #539131-1VL). Samples were then homogenized using a Qiagen TissueLyser LT at 50 oscillations/second for 30 s (x2). Following 30 min incubation at 4 °C, samples were centrifuged at 12,000 RPM for 15 min at 4 °C. Supernatants were collected and stored at −80 °C until the time of the experiment. A bead-based multiplex assay for protein detection was used to quantify expression of GM-CSF, IFN-γ, IL-10, IL-13, IL-1β, IL-2, IL-4, IL-5, IL-6, IL-7, IL-8, IL-12 (p70), and TNF-a (MilliporeSigma, HSTCMAG28SPMX13). Data were graphed in GraphPad Prism 7 and statistics were determined using Welch's *t*-test where $p \leq 0.05$*, $p \leq 0.01$**, $p \leq 0.001$***, and $p \leq 0.0001$****. Samples with values that were too low to be extrapolated from the standard curve were assigned a value of 0.01.

2.6. Mouse model of Aspergillus keratitis and RNA isolation from infected corneas and EMEM

6–8 wk old, male C57BL/6 J mice (Jackson Laboratory) were immunosuppressed with 100 mg/kg methylprednisolone intraperitoneally (i.p.) on the day preceding fungal inoculation. On the day of inoculation, *A. fumigatus* (strain Af293) conidia were incubated in YPD broth (yeast extract, peptone, glucose) at a density of 1.0×10^5 conidal/mL and incubated for 4 h until in shaking culture at 35 °C until conidia were swollen, but not polarized. The swollen conidia were collected via centrifugation, washed with PBS (2X), and resuspended in ~0.5 mL PBS. This served as the inoculum. To infect mice, animals were anesthetized with 100 mg/kg ketamine and 6.6 mg/kg xylazine i.p., and the corneal epithelium over the pupil of the right eye was removed with an algerbrush II. 5 μl of fungal inoculum were topically applied over the abraded cornea and remained in place for 20 min before being removed with a kim wipe. The left eye remained untouched as a control and in accordance with the Association for Research in Vision and Ophthalmology (ARVO) guidelines for the use of animals in vision research. Animals were monitored twice daily until 48 h post-inoculation, at which point animals were photographed, and the eyes were removed following euthanasia under IACUC-approved procedure. The corneas were resected and pooled (4–9 corneas per group), placed in TriZol, and homogenized with 0.5 mm glass beads (same procedure as for the 3D constructs above).

For the EMEM culture samples, conidia (harvested as described above) were inoculated into serum-free, antimycotic-free EMEM (PurMabiologics) to a density of 6.74×10^4/mL, the same density used for the 3D constructs. 3 mls of the inoculated media were added to a 6-well plate (Thermo Scientific). Following 48 h incubation at 35 °C, 5% CO_2, the media was aspirated for the well and the fungal biomass was collected with a spatula, dried on filter paper, and added to a microcentrifuge tube containing 100 μl of 0.1 mm glass beads (Biospec Products) and 1 mL Trizol for RNA extraction as describe above.

2.7. qRT-PCR

For quantitative PCR analysis, extracted RNA (described above) was reverse transcribed into cDNA following the manufacturer's protocol for the SuperScript II First-Strand cDNA Synthesis kit. qPCR was performed using either TaqMan (Applied Biosystems, Foster City) of GAPDH (Hs99999905_m1) or Luna Universal qPCR mastermix (SYBR green; NEB) as indicated. All primers used in the study are listed in Table S2. Fold-expression changes were calculated using the $2^{\Delta\Delta Ct}$ method and analyzed using Graph Pad Prism 9.0.1 and MS-Excel.

2.8. Transmission electron microscopy (TEM)

The constructs were washed twice with PBS and fixed after their indicated time points in 4% paraformaldehyde, 2% glutaraldehyde, and 0.1 M sodium cacodylate fixative for 4 h at 4 °C and processed for TEM following standard procedures that have been previously described (Gipson et al., 1983). Cell constructs were fixed with 4% Paraformaldehyde (EM grade), 2.5% Gluteraldehyde (EM grade), in 0.1 M Sodium Cacodylate buffer for 16 h at 4 °C. Samples were then post fixed for 90 min in 1% Osmium tetroxide (OsO4) in 0.1 M Sodium Cacodylate, and rinsed three times for 5 min each in 0.1 M Sodium Cacodylate buffer. The cell constructs were then dehydrated in a sequential acetone series including 50%, 60%, 75%, 85%, 95%, 100%; the samples were in each a for 15 min shaking at RT. Then the samples were then treated 100% Propylene Oxide for 15 min (x2). Following dehydration, the

samples were infiltrated in a graded Epon/Araldite (EMS) resin/Propylene Oxide series (1:3, 1:1, 3:1) for 60 min, overnight, and 120 min the next day respectfully. The cell constructs were further infiltrated with pure resin for 45 min, 90 min, and then overnight. The samples were then embedded in resin plus BDMA (accelerator) and polymerized at 60 °C for 48 h. Semi-thin sections were stained with toluidine blue and were imaged on a Zeiss Axiovert 200 M microscope.

2.9. Histology

Control and infected constructs were washed twice with PBS and fixed with 10% neutral buffered formalin for 24 h. The fixative was then removed and the constructs were placed in 70% ethanol until further processed. For sectioning, fixed constructs were placed on dental wax and cut into 5 μm thick sections while still attached to the polycarbonate membrane. The sections were then stained with toluidine blue as a general stain; Grocott-Gomori's methenamine silver (GMS) or Periodic acid Schiff-hematoxylin (PASH) stain was used to specifically visualize the fungal cell wall.

3. Results

3.1. Development of a 3D in vitro model of FK to probe the fungal-fibroblast interaction

As described above, we reasoned that the 3D stromal model developed by Karamichos and colleagues could serve as an ideal system to probe host-fungal interactions during FK. Before we could focus on such interactions, however, we first needed to establish that the model would generally mimic features of the disease, namely fungal invasion of and damage to the ECM. We therefore began by characterizing these baseline characteristics with the mold *F. petroliphilum*, a common agent of FK among contact lens wearers, particularly in the United States.

The experimental workflow is summarized in Fig. 1A and began with the generation of stromal constructs as previously described (Karamichos et al., 2010). Briefly, HCFs were isolated from healthy donor corneas, expanded in culture, and seeded onto 6-well polycarbonate inserts at a density of 1.0×10^6 cells/well. The plates were then cultured for four weeks in the presence of ascorbic acid (vitamin C) to promote matrix secretion by the cells. At the end of this incubation period, constructs of approximately 20 μm and 4–5 layers of HCFs thick were observed (Fig. 1B). The constructs were next overlaid with 5.0×10^4 conidia (spores) of *F. petroliphilum*. In an initial experiment, the fungal inoculum was prepared in tissue culture medium (EMEM), however, we noted that the spores germinated and formed a thick biofilm within the medium, rather than attaching and growing into the stromal constructs as desired (data not shown). Accordingly, we subsequently prepared the inocula in PBS, thus making the construct ECM the primary nutrient source for the fungus; EMEM (without serum or antimycotic) remained in the lower chamber of the transwell post-inoculation as a source of nutrients for the fibroblasts. Using this setup, we performed an initial time course and found that *Fusarium* conidia had partially germinated at 24 h post-inoculation and the construct ECM was largely intact (Figure S1). At 48 h, by contrast, the conidia had more fully developed into short hyphae and the constructs appeared degraded relative to un-infected controls (Fig. 1B). This suggested the fungus is able to invade the stromal matrix comparable to an *in vivo* infection. As these were the minimal requirements for pursuing this model, we next turned our attention to the fibroblasts.

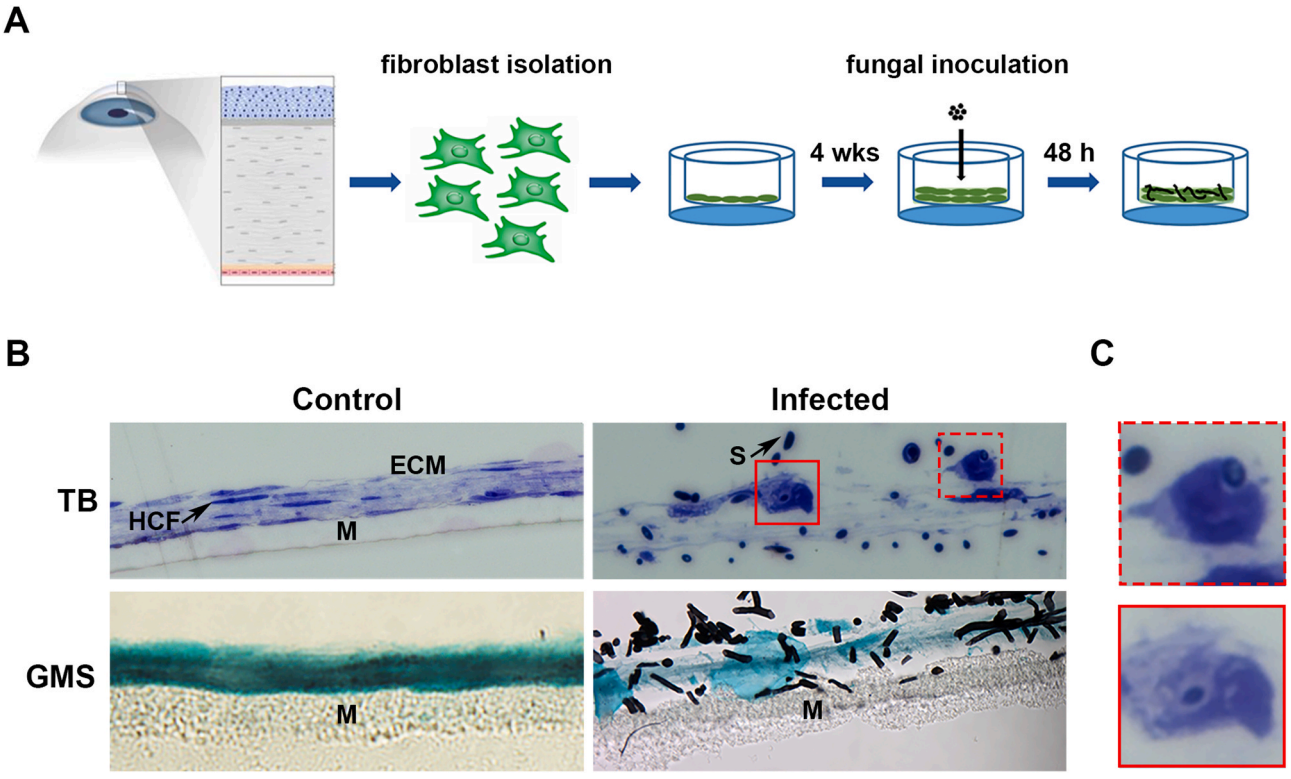

Fig. 1. Development of an *in vitro* 3D stromal model for fungal keratitis. **A)** 3D stromal constructs are generated following the isolation of HCFs from healthy human donors and culturing on a transwell membrane for up to 4 weeks. On the day of inoculation, the media in the upper chamber is replaced with the fungal spore inoculum prepared in PBS. **B)** Brightfield images demonstrating healthy and Fusarium-infected constructs at 48 h post-inoculation. Toluidine Blue (TB) is used to show all features of system, including the human corneal fibroblasts (HCF), the collagen extracellular matrix (ECM), the fungal spores (S), and the nylon membrane (M). Grocott-Gomori's methanamine silver (GMS) stain is used to stain fungal cell wall black. **C)** Close up image from panel B, demonstrating fibroblasts that have apparently internalized fungal spores. (For interpretation of the references to colour in this figure legend, the reader is referred to the Web version of this article.)

3.2. HCFs can engulf and internalize Fusarium conidia

Compared to the flat appearance of the HCFs in the control constructs, the cells often appeared thicker or more rounded in the *Fusarium*-infected samples (Fig. 1B). Fungal conidia contacted the surface of these fibroblasts and, in some cases, appeared to be internalized within them (Fig. 1C). We then imaged these constructs by transmission electron microscopy (TEM) to observe this interaction more closely. Within such images, the fibroblasts were readily distinguishable from conidia, the latter of which are ovoid/circular in shape and surrounded with an electron-dense cell wall (Figure 2A and 2B). TEM confirmed a direct fungal-fibroblast interaction as conidia were observed within distinct endomembranes. Remarkably, several HCFs appeared to have formed membrane/cytoplasmic projections that engulfed conidia otherwise not in contact with the primary cell body (Fig. 2C). Taken together, these data suggest that corneal fibroblasts have the capacity to detect and endocytose *Fusarium* conidia.

3.3. HCFs become pro-inflammatory in response to Fusarium infection

To elucidate the HCF response to *Fusarium* more fully, we performed Illumina sequencing of total RNA isolated from control (un-infected) and *Fusarium*-infected constructs at 48 h post-inoculation (n = 4/group). A total of 12,198 and 11,314 HCF genes with at least one normalized read were detected in the control and infected groups, respectively; the full dataset containing all detected genes and their RPKM values can be found in Table S1. Differentially expressed genes (DEGs) were considered to be those with at least 10 normalized reads in the control or infected groups and at least a 4-fold expression ($q \leq 0.01$) difference between the two groups. Based on these criteria, 156 genes were downregulated in the infected samples relative to the controls. The 30 genes with the strongest down-regulation are shown in Table 1 and include several with a described role in cell-growth or differentiation. Pathway enrichment analysis (KEGG) demonstrated that genes involved in metabolism, proteasome function, glycolysis/gluconeogenesis, and amino acid biosynthesis were statistically enriched among the entire downregulated gene list (Table 2). These results together suggest that growth and metabolism are largely repressed in HCFs following *Fusarium* infection.

A total of 396 genes were upregulated in the infected samples relative to the controls. Among the 30 genes with the greatest fold-induction, 10 were cytokines/chemokines with a well-described role in the inflammatory cell recruitment (CXCL 1,2,3,8) and activation (CSF-1, CSF-2, CSF-3, IL-11, IL-6, IL1α, IL1β, LIF) (Table 3). KEGG analysis demonstrated that IL-17 A, TNF, NFKB, C-type lectin, and Th17 signaling pathways were statistically enriched among the complete upregulated gene set, further supporting the interpretation that HCFs become pro-inflammatory in response to *Fusarium* infection (Table 4).

As a means to validate the pro-inflammatory transcriptional response, we next analyzed protein abundance of numerous cytokines and chemokines via a multiplexed immunoassay (Milliplex). Total protein was collected from control and *Fusarium*-infected constructs at 48 h post-inoculation, in parallel with the constructs harvested for transcriptomics (above). Several genes induced in the RNA-seq data set had corresponding probes in the Milliplex array and were similarly induced, including IL-1β, IL-6, IL-7, and IL-8 (also known as CSCL8) (Fig. 3). Several pro-inflammatory proteins were induced on the protein array that were not detected in RNA-seq data, including TNF-α, IL-2, and IL-13. We specifically followed up on TNF-α by qRT-PCR since the gene has previously shown to be induced in infected patient or murine FK corneas (Chidambaram et al., 2017; Zhang et al., 2020). In agreement with the protein results, TNF-α did demonstrate an induction in the qRT-PCR assay, perhaps reflecting a greater sensitivity over RNA-seq. IL-6, which is similarly known to be induced in FK corneas and

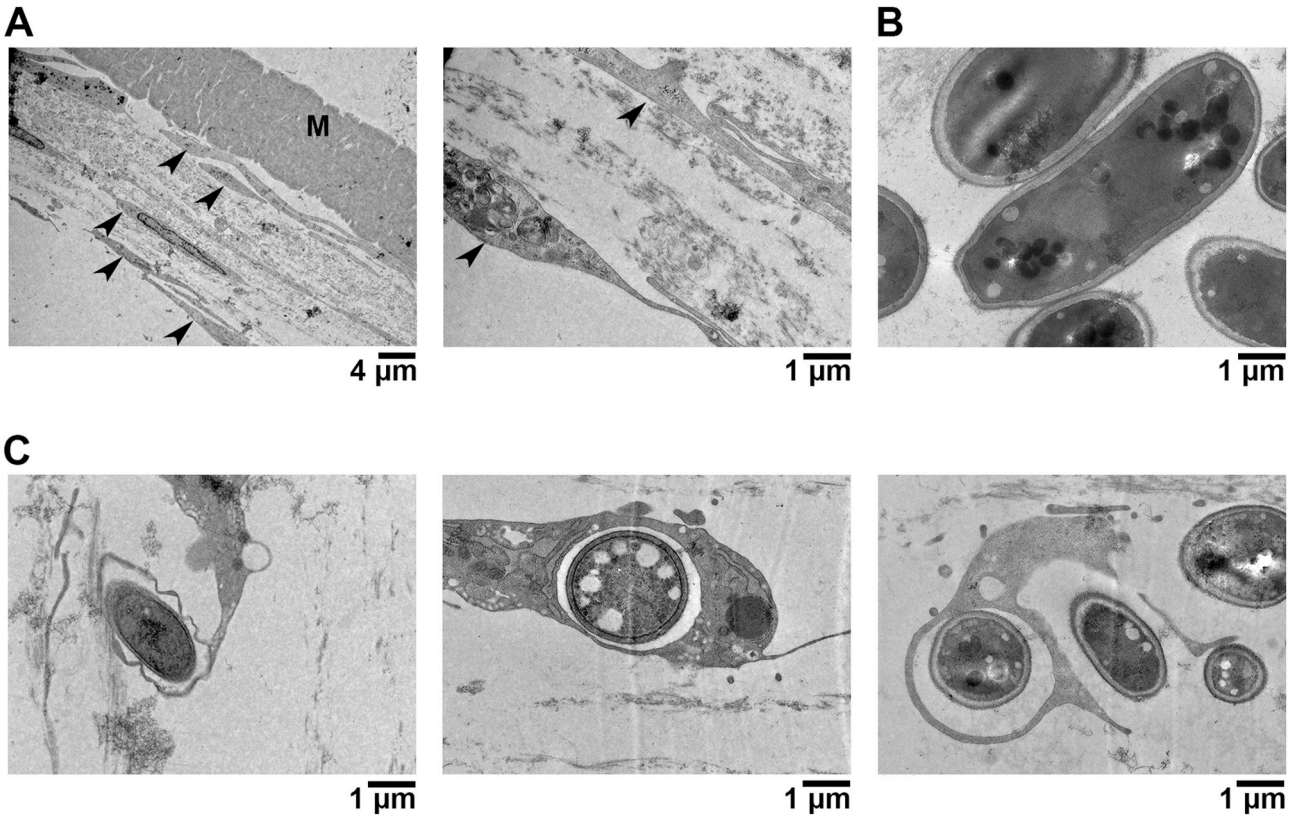

Fig. 2. Transmission Electron Microscopy (TEM) of Fusarium infected HCFs. **A)** Uninfected (control) constructs highlighting the flat apparencu of HCFs (arrowheads) and intact cellular matrix. **B)** Images of *Fusarium* microconidia, which are smooth and have an electron-dense cell wall. C) Infected constructs demonstrating an internalization of conidia within HCF endomembranes or cytoplasmic projections.

Table 1
Top 30 downregulated genes in *Fusarium*-infected HCFs based on fold-change compared to uninfected controls.

Gene	Description	Fold change	p value
EAPP	E2F-associated Phosphoprotein that promotes proliferation	−27.9098	.00005
CDC123	Cell Division Cycle 123 protein required for entry into S phase	−18.3722	.00005
AKR1C3	Aldo-keto reductase family 1 member C3	−15.7936	.00005
TXNDC9	Thioredoxin domain-containing protein involved in proliferation	−15.4993	.00005
C10orf10	also called DEPP1 involved in regulating autophagy	−13.1128	.00005
AKR1B10	Aldo-keto reductase family 1 member B10	−11.5138	.00005
AHNAK2	Nucleoprotein	−10.5996	.00005
ADH1B	Alcohol dehydrogenase 1 B	−9.87931	.00005
TSEN15	tRNA splicing endonuclease	−9.86378	.00005
PSMB6	Proteasome subunit beta type-6	−9.78533	.00005
TSNAX	Translin Associated Factor X involved in activation of the RNA-induced silencing complex	−9.56424	.00005
ABHD10	Abhydrolase Domain Containing 10	−9.54715	.00005
EHD3	EH Domain Containing 3	−9.48107	.00005
TXNIP	Thioredoxin Interacting Protein	−9.01758	.00005
FIBIN	Fin Bud Initiation Factor	−8.98376	.00005
SLC1A5	Soluble Carrier Family 1 Member 3 encodes a sodium-dependent neutral amino acid transporter	−8.91757	.00005
CBR1	Carbonyl reductase 1	−8.45052	.00005
GAS1	Growth Arrest Specific 1 involved in growth suppression	−8.31952	.00005
ZFYVE21	Zinc Finger FYVE-Type Containing 21 involved in cell adhesion	−8.15068	.00005
TRAPPC1	Trafficking Protein Particle Complex 1 involved in ER to Golgi transport	−8.1408	.00005
THYN1	Thymocyte Nuclear Protein 1 potentially involved in the induction of apoptosis	−8.07952	.00005
PITX2	Paired Like Homeodomain 2 encoding a transcription factor that regulates eye development	−7.90015	.00005
TNRC18	Trinucleotide Repeat Containing 18	−7.81345	.00005
UQCR10	Ubiquinol-Cytochrome C Reductase involved in respiratory metabolism	−7.60601	.00005
PSAT1	Phosphoserine Aminotransferase 1	−7.57891	.00005
MRPS17	Mitochondrial Ribosomal Protein S17	−7.52802	.00005
LRIG3	Leucine Rich Repeats and Immunoglobulin Like Domain	−7.36012	.00005
ZFHX4	Zinc Finger Homeobox 4	−7.2105	.00005
PREB	Prolactin Regulatory Element-Binding Protein	−7.18451	.00005
FBXO38	F-Box Protein 38	−7.18292	.00005

Table 2
KEGG analysis of the 156 downregulated genes in *Fusarium*-infected HCFs.

Name	p-value	Genes
Metabolic Signaling	2.89e-04	AKR1C3,AKR1B10,ADH1B,CBR1,UQCR10, PSAT1,ALDH3A2, GCLM,ADH5,IDH1,NDUFV3,CHPF2,NDUFA9, PDE5A,CAT,RDH10,MAT2B,ASNS, MGAT2, UROD, SACM1L,PDHB,PCK2,NDUFA12, EPRS, AGPS,RPE,ADCY7,HIBADH,NQO1
Proteosome	4.39e-03	PSMB6,PSMA3,PSMB3,PSMA4,PSMC2
Glycolysis/ Gluconeogenesis	3.17e-02	ADH1B,ALDH3A2,ADH5,PDHB,PCK2
Biosynthesis of Amino Acids	5.00e-02	PSAT1,IDH1,MAT2B,ASNS,RPE

Table 3
Top 30 upregulated genes in *Fusarium*-infected HCFs based on fold-change compared to uninfected controls.

Gene	Description	Fold change	p value
HSPA6	Heat Shock Protein Family A (Hsp70) Member 6	1,794	.00005
CXCL8	chemokine involved in neutrophil recruitment and angiogenesis	1,496	.00005
CSF3	cytokine involved in granulocyte production and function	1,308	.00005
CXCL2	chemokine involved inflammation and angiogenesis	895	.00005
CXCL3	chemokine involved in neutrophil recruitment and angiogenesis	651	.00005
C11orf96		537	.00005
TNFAIP3	TNF-α induced protein that inhibits NF-kappa-B activation and TNF-mediated apoptosis	420	.00005
FOSB	Fos proto-oncogene, AP-1 transcription factor subunit implicated in cell proliferation and differentiation	388	.00005
HSPA1A	Heat Shock Protein (Hsp70) family member	263	.00005
IL11	Gp130 cytokine family member that play a role in T-cell-dependent development of B-cells	245	.00005
HSPA1B	Heat Shock Protein (Hsp70) family member	213	.00005
TFPI2	Kunitz-type serine proteinase inhibitor family	212	.00005
G0S2	G0/G1 switch 2	205	.00005
IL6	cytokine involved in inflammation and B cell maturation	199	.00005
MFSD2A	Sodium-dependent lysophosphatidylcholine transporter	184	.00005
DNAJB1	Heat Shock Family (Hsp40) member	151	.00005
BIRC3	IAP family member that inhibits serum-deprivation-induced apoptosis	144	.00005
LIF	Leukemia Inhibitory Factor, IL-6 family cytokine	123	.00005
NR4A3	Nuclear receptor subfamily 4 A member 3	91	.00005
IL1A	cytokine involved in inflammation and hematopoiesis	81	.00005
CXCL1	chemokine involved in neutrophil recruitment	70	.00005
NR4A2	Nuclear receptor subfamily 4 A member 2	68	.00005
CLDN14	Claudin 14 involved in cell-to-cell adhesion in epithelial and endothelial sheets	63	.00005
ATF3	mammalian Activation Transcription Factor/ CREB protein family of transcription factors	61	.00005
NFKBIA	NF-kappa-B inhibitor family	59	.00005
CD83	Immunoglobulin superfamily of receptors involved in the regulation antigen presentation	58	.00005
MMP1	M10 family of matrix metalloproteinases that breaks down interstitial collagens	57	.00005
NIPAL4	NIPA like domain containing membrane receptor	52	.00005
IL1B	cytokine involved in inflammation produced by activated macrophages	51	.00005
TRIM36	E3 ubiquitin-protein ligase	50	.00005

strongly induced in our RNA-seq data, was similarly induced in qRT-PCR and protein assays (Fig. 3A).

3.4. Several upstream regulators may contribute to the HCF pro-inflammatory response

We next used Ingenuity Pathway Analysis (IPA, Qiagen) to identify putative regulatory proteins involved in the HCF response to *Fusarium* infection. This software assesses the overlap between experimental (e.g. RNA-seq) data and an extensively curated database of target genes for each of several hundred known regulatory proteins. It then uses the statistical significance of the overlap and the direction of the differential gene expression to make predictions about activation or repression of these regulatory proteins and associated pathways.

We first focused on HCF cell surface proteins that might interact with the fungus directly to initiate the pro-inflammatory cascade. Of 104 annotated 'transmembrane' proteins in the IPA curation, 19 were predicted to be activated. These included well-known pathogen recognition

Table 4
KEGG analysis of the 396 upregulated genes in *Fusarium*-infected HCFs.

Name	p-value	Genes
IL-17 A Signaling	3.53e-17	HSP90AB1,MAPK6,TRAF4,CEBPB, JUND, CXCL6,MMP3,JUN, NFKB1,HSP90AA1,CXCL5,FOS,FOSL1, PTGS2,IL1B,MMP1, NFKBIA, CXCL1,IL6,FOSB, TNFAIP3,CXCL3, CXCL2,CSF3,CXCL8
TNF Signaling	4.93e-16	FAS,MAP2K3,CSF1,CEBPB,MAP3K8, ICAM1,CREB5,CXCL6,MMP3,JUNB,IRF1, JUN,NFKB1,TRAF1,CXCL5,FOS,PTGS2, IL1B,NFKBIA, CXCL1,LIF,BIRC3,IL6,TNFAIP3,CXCL3, CXCL2
NFκB Signaling	5.97e-8	TICAM1,PLAU, CYLD,ICAM1,NFKB2,RELB, NFKB1,TRAF1,PTGS2, GADD45B,IL1B,NFKBIA, CXCL1,BIRC3, TNFAIP3,CXCL3,CXCL2, CXCL8
MAPK Signaling	1.45e-12	HSPA8,FAS,MAP2K3,GADD45A, MAPKAPK2,CSF1,PPP3CC, HSPB1,DUSP10,VEGFA,MAP3K8,JUND, PLA2G4C,NFKB2,RELB, JUN,DUSP1,NFKB1,DUSP5,FOS,GADD45B, NR4A1,DUSP8,EREG, IL1B,IL1A,HSPA1B,HSPA1,HSPA6
C-type Lectin Receptor Signaling	7.18e-6	MAPKAPK2,CBLB,PLK3,PPP3CC,CYLD, EGR3,NFKB2,IRF1,RELB, JUN,NFKB1,PTGS2,IL1B,NFKBIA,IL6
Cytokine-cytokine Receptor Interaction	6.06e-5	FAS,ACKR3,CSF1,TNFRSF10B,CLCF1, TNFRSF12A,INHBA,IL6R,CXCL6,IL32,IL7, RELT, CXCL5,GDF15,IL1B,CXCL1,IL1A,LIF, IL6,IL11,CXCL3,CXCL2,CSF3,CXCL8
Th17 Cell Differentiation	2.89e-4	HSP90AB1,PPP3CC,RORA, NFKBIB,IL6R, JUN,NFKB1,HSP90AA1,NFKBIE,FOS,IL1B, NFKBIA,IL6
NOD-like Receptor Signaling Pathway	3.35e-4	HSP90AB1,TICAM1,NFKBIB, NAMPT, RIPK2,JUN,NFKB1, HSP90AA1,IL1B,NFKBIA, CXCL1,BIRC3,IL6, TNFAIP3,CXCL3, CXCL2,CXCL8
Apoptosis	5.45e-3	FAS,GADD45A,MCL1,ERN1,TNFRSF10B, JUN,NFKB1,PMAIP1, TRAF1,FOS,GADD45B,NFKBIA, BIRC3
Circadian Rhythm	1.27e-2	NR1D1,RORA, BHLHE41,PER1,CRY1, BHLHE40
Cellular Senescence	2.50e-2	MAP2K3,GADD45A,MAPKAPK2,PPP3CC, SIRT1,RASSF5,NFKB1,ETS1,SERPINE1, GADD45B,IL1A,IL6,CXCL8
Toll-like Receptor Signaling Pathway	3.22e-2	MAP2K3,TICAM1,MAP3K8,JUN,NFKB1, FOS,IL1B,NFKBIA,IL6, CXCL8

receptors (PRRs), including Dectin-1 (*clec7A*), TLR2, TLR3, TLR4, TLR5, TLR7, and TLR9. Each of these PRRs, however, share in common several downstream output genes (e.g. pro-inflammatory cytokines regulated by NF-kB) that are upregulated in infected samples. This redundancy creates a bias in the analysis that may lead to false-positives, i.e. proteins considered 'activated' by the software even though they are not involved biologically. Indeed, Dectin-1, TLR5 and TLR9 were not detected in either of control or infected RNA-seq datasets or by RT-PCR (data not shown), suggesting that HCFs may not express these proteins. By contrast, TLR3, TLR4, and TLR7 were detected by RNA-seq, but they were not induced in the infected samples relative to the controls. TLR2 was, however, upregulated in the infected samples, suggesting that this protein may detect fungal cell wall moieties (e.g. polysaccharides) to initiate the response. It should be noted, that TLR2 signal remained below 10 FPKM in both the control and infected datasets, indicating a low-level of expression overall.

At the pathway level, IPA demonstrated an enrichment of genes within the IL-17 A, IL-6, TNF-α receptor signaling, and auto-inflammatory pathways (Table 5). These cytokine pathways may play a key role in propagating the pro-inflammatory cascade downstream of the initial fungal detection event. Though IL-6 and TNF-α were induced in the infected constructs (Fig. 3), IL-17 A was not detected in the RNA-seq, nor was it induced at the protein level (Table S1 and data not shown).

3.5. *Fusarium* infection regulates HCFs expression of matrix remodeling proteins

As corneal fibroblasts secrete MMPs as part of their normal tissue function as well as in response to bacterial antigen, we predicted they may similarly up-regulate these proteins during fungal infection. Consistent with this prediction, RNA-seq revealed an upregulation of both *MMP1* and *MMP3* in infected samples relative to controls, and their induction at the protein level was confirmed by the Milliplex assay. *MMP9* was not detected in the RNA-seq dataset, but has been described as being highly induced in FK corneas; we, therefore tested its expression by qRT-PCR and found it was detectable and induced in infected constructs (Table S1 and Fig. 4A).

In contrast to the induction of MMPs, the RNA-seq data suggested a down-regulation of several genes encoding collagen components, including *COL1*, *COL3*, and *COL5*. The reduced expression of these genes was confirmed by qRT-PCR (Fig. 4A). Taken together, these data indicate that *Fusarium* infection broadly regulates the expression of matrix remodeling genes, including those encoding MMPs and collagen, ultimately favoring a state of collagen degradation.

3.6. *A. fumigatus* similarly induces a pro-inflammatory and pro-fibrotic in HCFs

To determine if the model is suitable for other fungal pathogens, we performed a similar experimental workflow for another common FK agent, *Aspergillus fumigatus*. Using the same inoculation parameters as above, we found that *A. fumigatus* infected constructs faster than *F. petroliphilum*, with hyphae present by 12 h and matrix damage appreciable by 24 h post-inoculation (Figure S1). We performed qRT-PCR and Milliplex assays at 48 h, however, to keep the time points consistent between the two organisms. As with *Fusarium*-infected constructs, *Aspergillus* similarly induced the upregulation of selected pro-inflammatory cytokines and chemokines, including IL1B, IL6, IL7 and IL8. MMP1 was statistically induced at the level of mRNA and showed the same trend, although not significant, for the protein (Figure 5B and 5C). Taken together, these data suggest that the fibroblast response may be similar across fungi, and that the 3D model can be used to compare growth/infection kinetics of different pathogens.

3.7. *A. fumigatus* upregulates the expression of secreted collagenase genes during infection of stromal constructs

Standard host-pathogen co-culture models take place in tissue culture medium, which contains free glucose and amino acids for nutrition. Compared to such a system, we hypothesized that the ECM of the 3D constructs would more closely mimic the nutritional environment of an *in vivo* cornea, as we have previously shown with other corneal conditions including keratoconus and diabetic keratopathy (Priyadarsini et al., 2016). To provide some insight into this, we tested the expression of four *A. fumigatus* protease/collagenases (*mep*, *alp1*, *dppIV*, *dppV*) from fungus isolated from three conditions: (1) serum-free EMEM, which reflects the media used in standard culture models, (2) infected mouse corneas, and (3) the 3D stromal constructs. For the corneal infections, 6 week-old C57BL/6 mice were immunosuppressed with steroids on the day preceding infection. To initiate disease, the corneas were abraded and germinated (swollen) conidia were topically applied. Corneas of the infected animals were then isolated at 48 h post-inoculation, which corresponded to the same time point as the two *in vitro* conditions. Three separate corneal pools (4–9 corneas each) were assessed in the

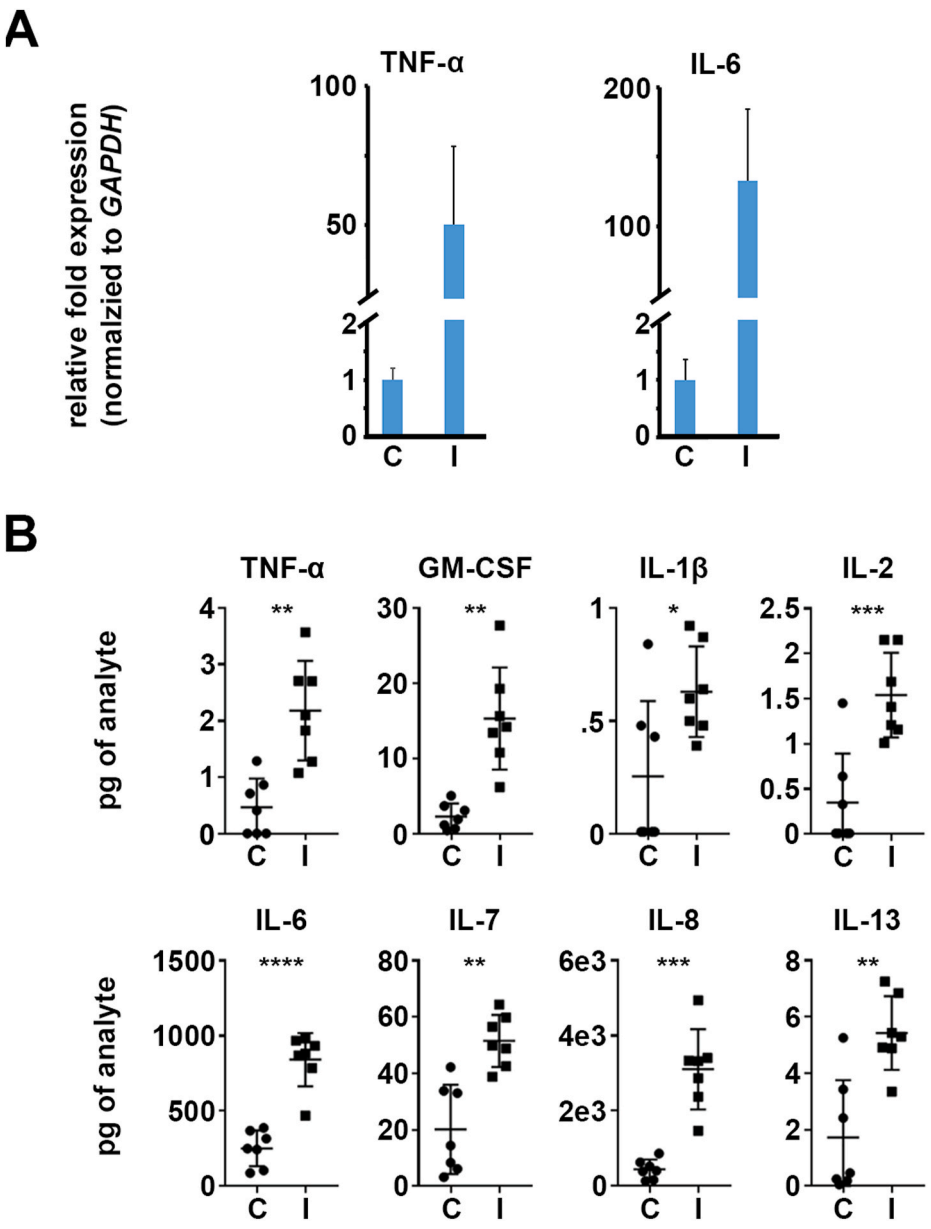

Fig. 3. HCFs become pro-inflammatory during fungal infection. **A)** qRT-PCR data demonstrating an upregulation of TNF-alpha and IL-6 in *Fusarium*-infected (I) constructs relative to the uninfected controls (C). GAPDH is used as the internal normalizer for each sample; data plots reflect the ratio of the infected samples relative to the control (set to '1'). **B)** Protein quantitation assay (Milliplex) demonstrating an upregulation of pro-inflammatory cytokines and chemokines.

Table 5
Upregulated signaling pathways in *Fusarium*-infected HCFs based on Ingenuity Pathway Analysis.

Name	p-value	Overlap
IL-17 A Signaling in Fibroblasts	1.09E-14	37.1% (13/35)
Role of IL17-A in Arthritis	1.84E-14	27.3% (15/55)
IL-6 Signaling	5.80E-14	15.9% (20/126)
Role of Macrophages, Fibroblasts and Endothelial Cells in Rheumatoid Arthritis	1.45E-12	8.9% (28/313)
TNFR2 Signaling	1.49E-12	36.7% (11/30)

experiment. Relative to the EMEM condition, we found an upregulation of *alp1* (avg. 233-fold), *mep* (avg. 539 fold), and *dppIV* (avg. 9-fold) in infected corneas, indicating the cornea does represent a protein-rich environment to which the fungus must adapt (Figure S2). In the 3D constructs, we found a significant induction of *dppIV* (avg. 5-fold) and *dppV* (avg 10-fold), but not of *alp1* and *mep* (Fig. 5D). This suggests that the 3D constructs do promote a similar, although not an identical, induction of proteases to that observed in the infected *in vivo* cornea.

4. Discussion

In vivo models of FK generally capture all of the salient features of the disease, including the pathogen and a myriad of host cell populations interacting within and damaging the corneal tissue. *In vitro* (co-culture) models, by contrast, allow for the study of specific host cell responses to the fungus, but lack the appropriate physiological environment to explore much else. A 3D fibroblast model developed by Karamichos

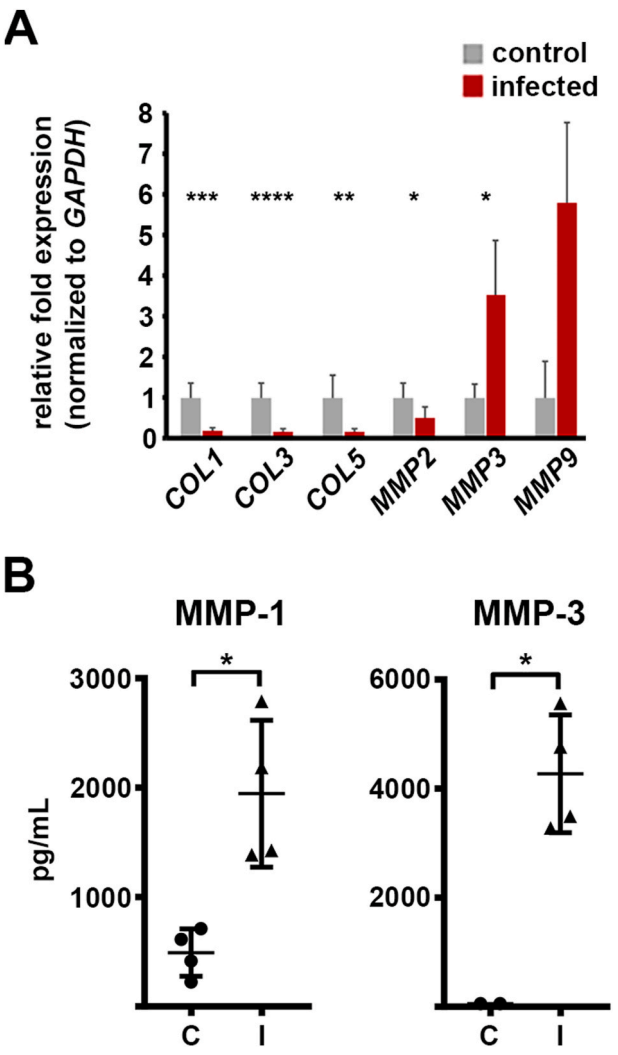

Fig. 4. Altered expression of matrix remodeling genes during *Fusarium* infection. **A)** qRT-PCR data demonstrating an differential regulation of various collagen (*COL*) and matrix metalloproteases (MMP)-encoding genes in infected (I) constructs relative to the un-infected controls (C). GAPDH is used as the internal normalizer for each sample; data plots reflect the ratio of the infected samples relative to the control (set to '1'). **B)** Protein quantitation assay (Milliplex) demonstrating an upregulation of MMP-1 and MMP-3 in Fusarium-infected HCF constructs.

et al. contains a fibroblast-secreted ECM and has been used to study a variety of physiologic and disease states of the stroma, including corneal fibrosis, corneal diabetes, keratoconus, UV-crosslinking, and cell-cell communication (Priyadarsini et al., 2016; Sharif et al., 2019; McKay et al., 2019; Karamichos et al., 2010). We reasoned that the system could be co-opted as a model for FK that would allow both fibroblast biology to be explored in parallel with fungal growth and penetration kinetics, which would make it the first of its kind. We tested these features of the model with two common mold agents of FK, *F. petroliphilum* and *A. fumigatus*.

Considering the host cells first, our data agree with previous studies that demonstrate cultured corneal fibroblasts become pro-inflammatory upon challenge with fungal antigen. Li et al. for example, challenged immortalized HCFs (2D culture) with heat-killed *A. fumigatus* hyphae and found induction of *IL6* and *IL8* mRNA (Li et al., 2013). We observed the same upregulation of these markers at both the gene and protein level when our constructs were challenged with live *A. fumigatus* or *F. petroliphilum*. Indeed, pro-inflammatory cytokines and chemokines were among the most strongly upregulated genes in *Fusarium*-infected constructs based on RNA-seq, and pro-inflammatory pathways (IL-17, TNF, NFkB, MAPK, TLR) were all statistically enriched within the induced gene category. In line with this analysis, Nomi and colleagues directly demonstrated NFkB and MAPK pathways are activated in HCFs by zymosan. Zymosan is purified fungal β,1–3 glucan and is a known agonist for both Dectin-1 (c-type lectin) TLR2. These two receptors co-localize and synergize within macrophage phagosomes to drive the NF-kB mediated pro-inflammatory response and several lines of evidence have implicated their importance in FK (Choi et al., 2011; Li et al., 2019; Zhong et al., 2016). First, both the mRNA and protein for Dectin-1 and TLR2 are upregulated in fungal-infected corneal epithelial cells *in* vitro as well as whole mouse corneas *in vivo* (Jin et al., 2007; Kolar et al., 2017; Guo et al., 2012; Wu et al., 2015; Zhao et al., 2009; Karthikeyan et al., 2011). Second, inhibition of either gene results in attenuated corneal opacity and inflammatory signaling in one or more models of FK (Jin et al., 2007; Leal et al., 2010). Consistent with these observations, IPA analysis of our RNA-seq data indicated that both TLR2 and Dectin-1 (CLEC7A) were activated in *Fusarium*-infected HCFs; this was based on the upregulation of known downstream genes within our data set, including the NFkB signaling complex. The *TLR2* gene itself did indeed demonstrate an induction in *Fusarium*-infected constructs. By contrast, however, *CLEC7A* was not detected in either infected or control samples, nor were genes involved in the proximal Dectin-1 signaling module, including Src kinase, Syk kinase, or Card9. Taken together, these data suggest that fungal β-glucan may activate corneal fibroblasts exclusively through the TLR2-NFkB signaling module.

A previously unreported activity of HCFs in our study is the direct internalization of fungal conidia. Although fibroblasts are not "professional" phagocytes, the uptake and turnover of damaged ECM particulate is an important function of these cells at the site of corneal injury. Indeed, the ability of cultured HCFs to take up beads has been described for decades and, most recently, Sato et al. demonstrated this rate of phagocytosis increases following stimulation with plasminogen (Lande et al., 1981; Sato et al., 2019). Whether the uptake of *Fusarium* conidia we captured reflects stochastic phagocytic activity of the cells or a stimulated response (e.g. through direct interaction with the fungus or damaged ECM) is currently unclear. It is also unclear if endocytosed spores are killed by the HCF, or vice versa. Whereas the endosomes of macrophages become acidified and accumulate microbicidal compounds (e.g. ROS and hydrolases), to our knowledge, such killing capacity has not been demonstrated in corneal fibroblasts. Histological examination of resected corneas from FK patients suggests the fibroblasts are apoptotic at late stages of infection (Vemuganti et al., 2004); but their fate at early stages, i.e. prior to neutrophil infiltration, is unknown. The outcome of the fungal-fibroblast interaction is the topic of ongoing investigation in our group. In any case, our current data cumulatively support a model in which corneal fibroblasts serve as immune surveillance cells within the corneal stroma, similar to macrophages or dendritic cells, and can promote the recruitment of peripheral neutrophils through the expression of pro-inflammatory cytokines and chemokines. Pro-inflammatory signaling is likely exacerbated during early infection by fibroblast-derived MMPs, that can cleave IL-1β into the active form. Moreover, the MMPs may directly breakdown the ECM and promote both fungal invasion and leukocyte migration through the stroma.

Our results concerning fibroblast activity in the presence of microbial antigen is in agreement with studies performed in standard (2D) culture models. While this serves as an important validation of the 3D model, it raises an important question: what new information can the 3D model provide? We propose the answer is manifold, but ultimately relates to the presence of the fibroblast-derived collagen matrix. First, we were able to visualize hyphal penetration through, and degradation of, the ECM, which mimics the pathogenesis within FK corneas. Moreover, we observed that *A. fumigatus* collagenase genes were differentially upregulated in both the 3D construct and infected murine corneas, relative to tissue culture media (EMEM). Each of the tested protease

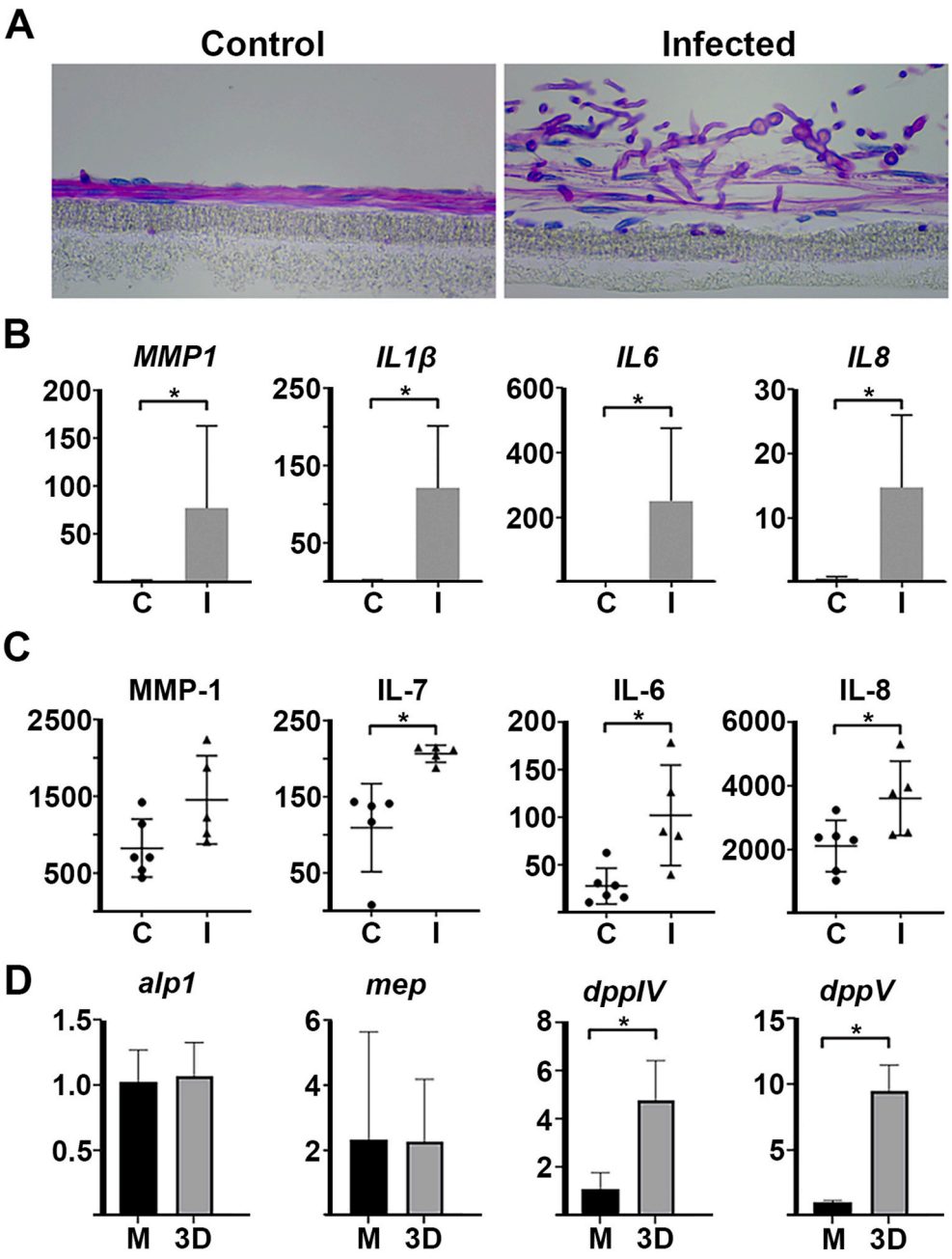

Fig. 5. Altered fibroblast and *Aspergillus* gene expression within the 3D model. **A)** Periodic Acid Schiff-hematoxylin (PASH) staining of control and *A. fumigatus*-infected constructs. Fibroblast nuclei stain blue and fungal cell walls stain pink. **B)** qRT-PCR data demonstrating the upregulation of pro-inflammatory cytokines, chemokines, and matrix metalloprotease genes in *Aspergillus*-infected (I) constructs relative to uninfected controls (C). **C)** Milliplex data demonstrating the upregulation of the corresponding proteins. **D)** qRT-PCR demonstrating the expression of several *A. fumigatus* collagenase genes grown in the 3D construct model relative to tissue culture media, EMEM media (M). Data for all panels and conditions taken at 48 h post-inoculation. (For interpretation of the references to colour in this figure legend, the reader is referred to the Web version of this article.)

genes were previously shown to be induced upon culture in proteinaceous media (Bergmann et al., 2009). We hypothesize that collagen and proteoglycans present in the 3D model and *in vivo* stroma represents the primary nitrogen source for the fungus and thereby drives a metabolic shift towards protein catabolism. EMEM, by contrast, contains free amino acids and glucose that likely suppress the expression of collagenase genes. Indeed, we noticed that *F. petroliphilum* invaded the stromal construct when the inoculum was prepared in non-nutritive PBS, but not EMEM. Since standard culture models take place in tissue culture media, we suggest that the 3D constructs represent a more physiologically relevant environment to probe fungal metabolic activities. Taken all the above observations together, the 3D construct model may represent an ideal platform to compare the stromal invasiveness (virulence) of various fungal species, or mutants of a particular species, e.g. with metabolic or protease defects. The antigenicity of a particular fungal strain could be assessed in parallel using fibroblast cytokine expression as a readout.

In summary, 3D stromal constructs provide the benefits of a typical *in vitro* system, e.g. more experimental control, but within a more physiologically relevant context. Beyond the experiments we have described, the model could easily be adapted to screen antifungal and anti-inflammatory characteristics of novel drugs or treatment modalities such as corneal collagen cross-linking (Sharif et al., 2019). The major disadvantages to consider with the model is the initial time needed (1 month) to cultivate the stromal constructs and the lack of additional corneal cells that are important in FK, such as epithelial cells (Jin et al., 2007; Kolar et al., 2017). Karamichos et al. have demonstrated that corneal epithelial and/or nerves can be added to this culture system, suggesting that the model can be fine-tuned based on the research question (McKay et al., 2019; Sharif et al., 2018).

Declaration of competing interest

None.

Acknowledgements

We would like to thank Linda Boone (DMEI Imaging Core), Mark Dittmar and staff (DMEI Animal Research Facility), and the staff at the Oklahoma Medical Research Foundation Imaging Core Facility for excellent technical assistance. This work was supported by a Research to Prevent Blindness (RPB) Career Development Award to KKF, a RPB Unrestricted Grant to Dean McGee Eye Institute, and a 5P30EY021725-10 from the National Eye Institute to the OUHSC Department of Ophthalmology. None of the funding sources were involved in any aspect of the study design, the collection or interpretation of the data, writing of the manuscript or the decision to publish.

Appendix A. Supplementary data

Supplementary data related to this article can be found at https://doi.org/10.1016/j.exer.2021.108581.

References

Bergmann, A., Hartmann, T., Cairns, T., Bignell, E., Krappmann, S., 2009. A regulator of *Aspergillus fumigatus* extracellular proteolytic activity is dispensable for virulence. Infect. Immun. 77, 4041–4050.

Bharathi, M.J., Ramakrishnan, R., Meenakshi, R., Padmavathy, S., Shivakumar, C., Srinivasan, M., 2007. Microbial keratitis in South India: influence of risk factors, climate, and geographical variation. Ophthalmic Epidemiol. 14, 61–69.

Chakravarti, S., Wu, F., Vij, N., Roberts, L., Joyce, S., 2004. Microarray studies reveal macrophage-like function of stromal keratocytes in the cornea. Invest. Ophthalmol. Vis. Sci. 45, 3475–3484. https://doi.org/10.1167/iovs.04-0343.

Chang, D.C., Grant, G.B., O'Donnell, K., Wannemuehler, K.A., Noble-Wang, J., Rao, C.Y., Jacobson, L.M., Crowell, C.S., Sneed, R.S., Lewis, F.M., Schaffzin, J.K., Kainer, M.A., Genese, C.A., Alfonso, Cheung, N., Nagra, P., Hammersmith, K., 2016. Emerging trends in contact lens-related infections. Curr. Opin. Ophthalmol. 27, 327–332. https://doi.org/10.1097/ICU.0000000000000280.

Chidambaram, J.D., Kannambath, S., Srikanthi, P., Shah, M., Lalitha, P., Elakkiya, S., Bauer, J., Prajna, N.V., Holland, M.J., Burton, M.J., 2017. Persistence of innate immune pathways in late stage human bacterial and fungal keratitis: results from a comparative transcriptome analysis. Front. Cell Infect. Microbiol. 7, 193. https://doi.org/10.3389/fcimb.2017.00193.

Choi, H.J., Kim, M.K., Ko, J.H., Lee, H.J., Jeong, H.J., Wee, W.R., Seong, S.Y., Akira, S., 2011. Effect of Toll-like receptor 2 and 4 of corneal fibroblasts on cytokine expression with co-cultured antigen presenting cells. Cytokine 56, 265–271. https://doi.org/10.1016/j.cyto.2011.07.004.

Doughty, M.J., Jonuscheit, S., 2019. Corneal structure, transparency, thickness and optical density (densitometry), especially as relevant to contact lens wear-a review. Contact Lens Anterior Eye 42, 238–245. https://doi.org/10.1016/j.clae.2018.11.014.

Fujita, H., Ueda, A., Nishida, T., Otori, T., 1987. Uptake of India ink particles and latex beads by corneal fibroblasts. Cell Tissue Res. 250, 251–255. https://doi.org/10.1007/BF00219069.

Fukuda, K., Kumagai, N., Yamamoto, K., Fujitsu, Y., Chikamoto, N., Nishida, T., 2005. Potentiation of lipopolysaccharide-induced chemokine and adhesion molecule expression in corneal fibroblasts by soluble CD14 or LPS-binding protein. Invest. Ophthalmol. Vis. Sci. 46, 3095–3101. https://doi.org/10.1167/iovs.04-1365.

Fukuda, K., Ishida, W., Fukushima, A., Nishida, T., 2017. Corneal fibroblasts as sentinel cells and local immune modulators in infectious keratitis. Int. J. Mol. Sci. 18, 1831. https://doi.org/10.3390/ijms18091831.

Gao, N., Kumar, A., Yu, F.S., 2015. Matrix Metalloproteinase-13 as a target for suppressing corneal ulceration caused by Pseudomonas aeruginosa infection. J. Infect. Dis. 212, 116–127.

Guo, X., Hutcheon, A.E., Melotti, S.A., Zieske, J.D., Trinkaus-Randall, V., Ruberti, J.W., 2007. Morphologic characterization of organized extracellular matrix deposition by ascorbic acid-stimulated human corneal fibroblasts. Invest. Ophthalmol. Vis. Sci. 48, 4050–4060. https://doi.org/10.1167/iovs.06-1216.

Guo, H., Gao, J., Wu, X., 2012. Toll-like receptor 2 siRNA suppresses corneal inflammation and attenuates Aspergillus fumigatus keratitis in rats. Immunol. Cell Biol. 90, 352–357. https://doi.org/10.1038/icb.2011.49.

Jin, X., Qin, Q., Tu, L., Zhou, X., Lin, Y., Qu, J., 2007. Toll-like receptors (TLRs) expression and function in response to inactivate hyphae of *Fusarium solani* in immortalized human corneal epithelial cells. Mol. Vis. 13, 1953–1961.

Karamichos, D., Guo, X.Q., Hutcheon, A.E., Zieske, J.D., 2010. Human corneal fibrosis: an in vitro model. Invest. Ophthalmol. Vis. Sci. 51, 1382–1388. https://doi.org/10.1167/iovs.09-3860.

Karamichos, D., Lakshman, N., Petroll, W.M., 2007. Regulation of corneal fibroblast morphology and collagen reorganization by extracellular matrix mechanical properties. Invest. Ophthalmol. Vis. Sci. 48, 5030–5037. https://doi.org/10.1167/iovs.07-0443.

Karthikeyan, R.S., Leal Jr., S.M., Prajna, N.V., Dharmalingam, K., Geiser, D.M., Pearlman, E., Lalitha, P., 2011. Expression of innate and adaptive immune mediators in human corneal tissue infected with Aspergillus or fusarium. J. Infect. Dis. 204, 942–950. https://doi.org/10.1093/infdis/jir426.

Kolar, S.S., Baidouri, H., McDermott, A.M., 2017. Role of pattern recognition receptors in the modulation of antimicrobial peptide expression in the corneal epithelial innate response to *F. solani*. Invest. Ophthalmol. Vis. Sci. 58, 2463–2472. https://doi.org/10.1167/iovs.16-20658.

Lande, M.A., Birk, D.E., Nagpal, M.L., Rader, R.L., 1981. Phagocytic properties of human keratocyte cultures. Invest. Ophthalmol. Vis. Sci. 20, 481–489.

Leal Jr., S.M., Cowden, S., Hsia, Y.C., Ghannoum, M.A., Momany, M., Pearlman, E., 2010. Distinct roles for Dectin-1 and TLR4 in the pathogenesis of *Aspergillus fumigatus* keratitis. PLoS Pathog. 6, e1000976 https://doi.org/10.1371/journal.ppat.1000976.

Leal Jr., S.M., Pearlman, E., 2012. The role of cytokines and pathogen recognition molecules in fungal keratitis - insights from human disease and animal models. Cytokine 58, 107–111. https://doi.org/10.1016/j.cyto.2011.12.022.

Li, W., Yan, J., Yu, Y., 2019. Geometrical reorganization of Dectin-1 and TLR2 on single phagosomes alters their synergistic immune signaling. Proc. Natl. Sci. USA 116, 25106–25114. https://doi.org/10.1073/pnas.1909870116.

Li, Y., Yang, H., Wu, X., 2013. Pretreatment with TLR2 and TLR4 ligand modulates innate immunity in corneal fibroblasts challenged with *Aspergillus fumigatus*. Invest. Ophthalmol. Vis. Sci. 54, 4261–4270. https://doi.org/10.1167/iovs.12-11504. PMID: 23633661.

Lightfoot, J.D., Fuller, K.K., 2019. CRISPR/Cas9-Mediated gene replacement in the fungal keratitis pathogen *Fusarium solani var. petroliphilum*. Microorganisms 7, 457. https://doi.org/10.3390/microorganisms7100457.

McKay, T.B., Karamichos, D., Hutcheon, A.E.K., Guo, X., Zieske, J.D., 2019. Corneal epithelial-stromal fibroblast constructs to study cell-cell communication in vitro. Bioengineering 6, 110. https://doi.org/10.3390/bioengineering6040110.

McClellan, S.A., Huang, X., Barrett, R.P., Lighvani, S., Zhang, Y., Richiert, D., Hazlett, L. D., 2006. Matrix metalloproteinase-9 amplifies the immune response to Pseudomonas aeruginosa corneal infection. Invest. Ophthalmol. Vis. Sci. 47, 256–264.

Mundra, J., Dhakal, R., Mohamed, A., Jha, G., Joseph, J., Chaurasia, S., Murthy, S., 2019. Outcomes of therapeutic penetrating keratoplasty in 198 eyes with fungal keratitis. Indian J. Ophthalmol. 67, 1599–1605. https://doi.org/10.4103/ijo.IJO_1952_18.

Montgomery, M.L., Fuller, K.K., 2020. Experimental models for fungal keratitis: an overview of principles and protocols. Cells 9, 1713. https://doi.org/10.3390/cells9071713.

Myrna, K.E., Pot, S.A., Murphy, C.J., 2009. Meet the corneal myofibroblast: the role of myofibroblast transformation in corneal wound healing and pathology. Vet. Ophthalmol. 12, 25–27. https://doi.org/10.1111/j.1463-5224.2009.00742.x.

Nomi, N., Kimura, K., Nishida, T., 2010. Release of interleukins 6 and 8 induced by zymosan and mediated by MAP kinase and NF-kappaB signaling pathways in human corneal fibroblasts. Invest. Ophthalmol. Vis. Sci. 51, 2955–2959. https://doi.org/10.1167/iovs.09-4823.

Priyadarsini, S., Sarker-Nag, A., Rowsey, T.G., Ma, J.X., Karamichos, D., 2016. Establishment of a 3D in vitro model to accelerate the development of human therapies against corneal diabetes. PloS One 11, e0168845. https://doi.org/10.1371/journal.pone.0168845.

Rosa, R.H., Miller, D., Alfonso, E.C., 2009. The changing spectrum of fungal keratitis in south Florida. Ophthalmology 101, 1005–1013. https://doi.org/10.1016/s0161-6420(94)31225-5.

Saha, S., Banerjee, D., Khetan, A., Sengupta, J., 2009. Epidemiological profile of fungal keratitis in urban population of West Bengal, India. Oman J. Ophthalmol. 2, 114–118. https://doi.org/10.4103/0974-620X.57310.

Sato, T., Sugioka, K., Kodama-Takahashi, A., Murakami, J., Saito, A., Mishima, H., Nishida, T., Kusaka, S., 2019. Stimulation of phagocytic activity in cultured human corneal fibroblasts by plasminogen. Invest. Ophthalmol. Vis. Sci. 60, 4205–4214. https://doi.org/10.1167/iovs.19-27736.

Sivak, J.M., Fini, M.E., 2002. MMPs in the eye: emerging roles for matrix metalloproteinases in ocular physiology. Prog. Retin. Eye Res. 21, 1–14.

Sharif, R., Priyadarsini, S., Rowsey, T.G., Ma, J.X., Karamichos, D., 2018. Corneal tissue engineering: an in vitro model of the stromal-nerve interactions of the human cornea. J. Vis. Exp. 24, 56308. https://doi.org/10.3791/56308.

Sharif, R., Fowler, B., Karamichos, D., 2019. Collagen cross-linking impact on keratoconus extracellular matrix. PloS One 13, e0200704. https://doi.org/10.1371/journal.pone.0200704.

Short, D.P., O'Donnell, K., Thrane, U., Nielsen, K.F., Zhang, N., Juba, J.H., Geiser, D.M., 2013. Phylogenetic relationships among members of the *Fusarium solani* species complex in human infections and the descriptions of *F. keratoplasticum* sp. nov. *and F. petroliphilum* stat. nov. Fungal Genet. Biol. 53, 59–70. https://doi.org/10.1016/j.fgb.2013.01.004.

Spadea, L., Maraone, G., Verboschi, F., Vingolo, E.M., Tognetto, D., 2016. Effect of corneal light scatter on vision: a review of the literature. Int. J. Ophthalmol. 9, 459–464. https://doi.org/10.18240/ijo.2016.03.24.

Sugioka, K., Kodama-Takahshi, A., Sato, T., Okada, K., Murakami, J., Park, A.M., Mishima, H., Shimomura, Y., Kusaka, S., Nishida, T., 2018. Plasminogen-dependent collagenolytic properties of staphylococcus aureus in collagen gel cultures of human corneal fibroblasts. Invest. Ophthalmol. Vis. Sci. 59, 5098–5107. https://doi.org/10.1167/iovs.18-24925.

Taylor, P.R., Roy, S., Meszaros, E.C., Sun, Y., Howell, S.J., Malemud, C.J., Pearlman, E., 2016. JAK/STAT regulation of *Aspergillus fumigatus* corneal infections and IL-6/23-stimulated neutrophil, IL-17, elastase, and MMP9 activity. J. Leukoc. Biol. 100, 213–222. https://doi.org/10.1189/jlb.4A1015-483R.

Thomas, P.A., Kaliamurthy, J., 2013. Mycotic keratitis: epidemiology, diagnosis and management. Clin. Microbiol. Infect. 19, 210–220. https://doi.org/10.1111/1469-0691.12126.

Vemuganti, G.K., Reddy, K., Iftekhar, G., Garg, P., Sharma, S., 2004. Keratocyte loss in corneal infection through apoptosis: a histologic study of 59 cases. BMC Ophthalmol. 4, 16. https://doi.org/10.1186/1471-2415-4-16.

Wu, J., Zhang, Y., Xin, Z., Wu, X., 2015. The crosstalk between TLR2 and NOD2 in *Aspergillus fumigatus* keratitis. Mol. Immunol. 64, 235–243. https://doi.org/10.1016/j.molimm.2014.11.021.

Zhang, Q., Zhang, J., Gong, M., Pan, R., Liu, Y., Tao, L., He, K., 2020. Transcriptome analysis of the gene expression profiles associated with fungal keratitis in mice based on RNA-Seq. Invest. Ophthalmol. Vis. Sci. 61, 32. https://doi.org/10.1167/iovs.61.6.32.

Zhao, J., Wu, X., Yu, F.S., 2009. Activation of Toll-like receptors 2 and 4 in *Aspergillus fumigatus* keratitis. Innate Immun. 15, 155–168. https://doi.org/10.1177/1753425908101521.

Zhong, J., Huang, W., Deng, Q., Wu, M., Jiang, H., Lin, X., Sun, Y., Huang, X., Yuan, J., 2016. Inhibition of TREM-1 and Dectin-1 alleviates the severity of fungal keratitis by modulating innate immune responses. PloS One 11, eo050114. https://doi.org/10.1371/journal.pone.0150114.

Zhu, W.-S., Wojdyla, K., Donlon, K., Thomas, P.A., Eberle, H.I., 1990. Extracellular proteases of Aspergillus flavus: fungal keratitis, proteases, and pathogenesis. Diagn. Microbiol. Infect. Dis. 13, 491–497. https://doi.org/10.1016/0732-8893(90)90081-6.